Aerosol Optical Thickness Measurement with Elevation-Scanning Lidar

PAVEL I. IONOV AND ANDREW K. MOLLNER

The Aerospace Corporation, Los Angeles, California

(Manuscript received 18 September 2014, in final form 30 March 2015)

ABSTRACT

High-accuracy measurement of aerosol optical thickness (AOT) τ_a with an elevation-scanning lidar is demonstrated and the results are compared with a collocated Cimel 318 sun photometer. Linear regression of the time-coincident data from a 2-week measurement campaign with the two instruments is found to be $\tau_a^{\text{lidar}} = (1.00 \pm 0.17)\tau_a^{\text{phot}} + (0.025 \pm 0.019)$ (1σ). The method proved to have sufficient accuracy to measure AOTs of 0.1–0.2 commonly seen in relatively clear atmosphere. The measurement is absolute and thus does not depend on any external calibration standards.

1. Introduction

Aerosols play an important role in the atmosphere, and a variety of remote sensing methods exist for their detection and characterization. The aerosol optical remote sensing methods can be subdivided into passive (Holben et al. 1998; Kokhanovsky and de Leeuw 2009) and active (Adam et al. 2007; Alados-Arboledas et al. 2011; Burton et al. 2013; Ferrare et al. 2006; Hair et al. 2008; Kano 1968; Müller et al. 2001, 2011; Shipley et al. 1983; Sroga et al. 1983) methods, with sun photometry (Holben et al. 1998) being the most relied on method for calibrating space-based passive sensors (Kahn et al. 2007; Kokhanovsky and de Leeuw 2009). Aerosol optical thickness [AOT; or aerosol optical depth (AOD)] is the value of primary interest measured by the passive instruments:

$$\tau_a = \int_0^\infty \alpha_a(z)\, dz. \tag{1}$$

It is a column integral (over altitude z) of aerosol extinction α_a that makes no distinction between the contributions from aerosol scattering and aerosol absorption.

Active remote sensing (e.g., lidar) has many attractive properties, such as the ability to make measurements in the absence of sunlight and to provide detailed range profile information. However, to perform this range-dependent inversion, at least two independent lidar signals have to be measured, or a relationship between attenuation (α) and backscatter (β) has to be assumed. This can be seen by examining the lidar equation, which expresses received signal power P_S as a function of range R, defined as

$$P_S(R) = \frac{K(R)}{R^2}\beta(R)\exp\left[-2\int_0^R \alpha(r)\, dr\right], \tag{2}$$

where both attenuation α and backscatter β are composed of the molecular and aerosol parts:

$$\alpha = \alpha_m + \alpha_a \quad \text{and} \tag{3a}$$

$$\beta = \beta_m + \beta_a. \tag{3b}$$

Term $K(R)$ is the instrument parameter (incorporating light collection efficiency and other parameters). For longer ranges $K(R)$ approaches $AEc\eta/2$ for a typical pulsed lidar, where A is the receiver aperture area, E is transmitter pulse energy, c is the speed of light, and η is the transmission of the optics train. At shorter ranges $K(R)$ becomes range dependent. The dependence is usually not known. Furthermore, it is sensitive to the lidar receiver-to-transmitter coalignment. On the other hand, where it is known, or is known to be constant, Eq. (2) can be equivalently expressed in terms of "range corrected" signal $S(R)$, defined as

$$S(R) = \ln\left[\frac{P_S(R)R^2}{K(R)}\right]. \tag{4}$$

Denotes Open Access content.

Corresponding author address: Pavel Ionov, The Aerospace Corporation, M2/253, P.O. Box 92957, Los Angeles, CA 90009-2957.
E-mail: pavel.ionov@aero.org

DOI: 10.1175/JTECH-D-14-00183.1

Substituting Eq. (2) into Eq. (4) and applying logarithm and differentiation, we get an alternative form of the lidar equation in terms of S:

$$\frac{dS(R)}{dR} = \frac{d\ln[\beta(R)]}{dR} - 2\alpha(R). \tag{5}$$

In this simplified form, the difficulty of inverting a single lidar measurement $S(R)$ into two unknowns, $\alpha(R)$ and $\beta(R)$, becomes especially clear. The so-called Klett method (Klett 1981) involves an assumed relationship between α and β of the form

$$L(R) = \frac{\alpha(R)}{\beta(R)}, \tag{6}$$

where L is the extinction-to-backscatter ratio (also known as lidar ratio). Equation (5) can be solved if the lidar ratio, $L(R)$, is either known for the altitudes of interest or can be assumed constant. While the molecular lidar ratio α_m/β_m is constant ($8\pi/3$ sr), the aerosol lidar ratio α_a/β_a is generally neither known nor can be assumed to be constant with altitude. The aerosol lidar ratio depends strongly on the distribution of the particle shapes, sizes, and composition, and can vary from 20 to 100 sr (Ansmann and Müller 2005). Mechanisms such as the settling and deposition of aerosols due to gravity and water condensation lead to variations in both aerosol concentration and composition as a function of altitude in a typical atmosphere. Thus, it has to be concluded that in order to invert lidar signal into two independent parameters, $\alpha(R)$ and $\beta(R)$, at least two independent measurements have to be made.

One approach is to distinguish molecular and aerosol lidar signals spectrally, by either high-spectral-resolution lidar (HSRL) (Burton et al. 2013; Shipley et al. 1983; Sroga et al. 1983) or Raman lidar (Alados-Arboledas et al. 2011; Ferrare et al. 2006; Muller et al. 2001, 2011). Both techniques are more challenging technically than a simple Mie/Rayleigh lidar, and Raman lidar in particular suffers from a reduction in signal because of a factor of about 30 (for rotational Raman) to about 100 (for vibrational Raman) reduction in scattering cross section. An alternative is elevation-scanning lidar (Adam et al. 2007; Bergant et al. 2004; Hamilton 1969), where a Mie/Rayleigh lidar measurement is repeated with different elevation angles θ. To perform an inversion, an assumption of a stratified atmosphere is made—that is, α and β are only functions of altitude, but not the horizontal position (Adam et al. 2007; Bergant et al. 2004; Hamilton 1969). With this assumption and the substitution $z = \sin(\theta)R$, Eq. (5) can be rewritten as

$$\frac{dS(z,\theta)}{dz} = \frac{d\ln[\beta(z)]}{dz} - \frac{2\alpha(z)}{\sin(\theta)}. \tag{7}$$

Thus, by making measurements for at least two angles, both α and β can, in principle, be recovered. In practice, the perfect atmospheric stratification assumption needed for Eq. (7) is easily destroyed by turbulence and local aerosol sources. Another difficulty of applying all of the above-mentioned approaches to the recovery of $\alpha(R)$ is that it is related to the derivative of the measured signal, as seen in Eq. (5). This places very stringent requirements on the signal-to-noise of the measurement, particularly in a typical clear atmosphere in the absence of smoke or volcanic eruption events. Under such normal clear condition, AOT is typically only 0.1–0.2 in the visible and UV, and even less in the near IR (Kokhanovsky and de Leeuw 2009; NASA 2014). In addition to relating to the derivative of the signal, $\alpha(R)$ is also related to the derivative of $\beta(R)$. In the case of the multiangle measurement approach, this makes $\alpha(R)$ extremely sensitive to even small deviations from perfect stratification. The above-mentioned difficulties were pointed out already by Spinhirne et al. (1980) and more recently by other research (for instance, Adam et al. 2007; Bergant et al. 2004; Kovalev et al. 2011), and there have been several efforts to improve the results obtained from angle-scanning methods (Kovalev et al. 2012; Pahlow et al. 2004; Sicard et al. 2002).

In this work, we have focused solely on deriving an accurate measurement of AOT, rather than vertical aerosol profiles, as was the goal of previous aerosol lidar work. In sun photometry an approach similar to an elevation-scanning lidar measurement is used for absolute calibration and is called the Langley plot (Adler-Golden and Slusser 2007). For a Langley plot to be valid, the aerosol layer must be horizontally uniform over the angles of measurement. However, this horizontal uniformity only applies to the total column attenuation of the aerosol (from the ground to space), not to the specific vertical structure of the aerosol layers. Rigorously, what is assumed is that the integral of Eq. (1) does not change if an inclined integration path is chosen. This weaker assumption is less affected by turbulent mixing and localized aerosol sources than the assumption of complete stratification for all altitudes required to recover attenuation and backscatter profiles from a multiangle measurement (Adam et al. 2007; Hamilton 1969). Since in sun photometry the Langley plot method relies on the earth rotation for elevation scanning, this makes it only practical for the instrument calibration in daytime conditions with a clear atmosphere that is stable over a long period of time.

In this paper we ask the questions, if the same weaker (integral) uniformity assumption can be used to recover AOT from an elevation-scanning lidar measurement and if it would result in precision comparable to a sun

photometer measurement. Because we are only interested in the AOT (total column), the analysis can be made under the less restrictive assumption that the total column integral of α_a, Eq. (1), is constant with the lidar pointing angle. No assumption with respect to β_a is required other than that the measurement altitude z_1 can be chosen such that $\beta_a(z_1)$ makes a negligible contribution to the total β. This results in a measurement technique that is insensitive to small-scale fluctuations in aerosol scattering caused by turbulence or local fluctuations in boundary layer height. Our results indicate that indeed lidar AOT derived with this approach has at least a comparable precision to the sun photometry.

2. Measurement concept

To invert the elevation-scanning lidar measurement, we will rewrite Eq. (5) in the integral form,

$$S(R) = \ln[\beta(R)] - 2\int_0^R \alpha(r)\,dr, \tag{8}$$

and make the assumption that the integral,

$$\int_0^{z_1} \alpha(z,\theta)\,dz, \tag{9}$$

is independent of angle. We will further choose an altitude z_1 that is sufficiently high that essentially all the aerosols can be assumed to lie below and that $\beta_a(z_1)$ is either negligible or at least its variation with the pointing angle is negligible with respect to $\beta_m(z_1)$. With these assumptions Eq. (8) can be rewritten as

$$S(z_1,\theta) = \ln[\beta_m(z_1)] - 2\frac{\tau_m(z_1)+\tau_a}{\sin(\theta)}, \tag{10a}$$

where

$$\tau_m(z_1) = \int_0^{z_1} \alpha_m(z)\,dz. \tag{10b}$$

Since in practice, the absolute calibration of a lidar is not known, $S(z,\theta)$ is only known to a calibration coefficient. At the same time, β_m only depends on the atmospheric density, and thus it does not appreciably change during a typical measurement. To obtain AOT we perform a linear regression of $S(z,\theta)$ against air mass, $1/\sin(\theta)$, as an independent variable according to the model:

$$S(z_1,\theta) = C - 2\frac{\tau_m(z_1)+\tau_a}{\sin(\theta)}, \tag{11}$$

where C is a constant for a given measurement. As in sun photometry, τ_a is obtained from the slope by noting that the Rayleigh optical density $\tau_m(z_1)$ can be found from the standard atmosphere (with correction for ground-level atmospheric pressure) or weather/climate data when available. Since $\tau_m(z_1)$ depends only on the molecular density in the partial column from ground z_0 to z_1, $\tau_m(z_1)$ only depends on the pressure difference, $p(z_0) - p(z_1)$. When we examine radiosonde data from nearby (<250 km) weather stations for the month of February 2013, pressure at 15 km varied (1σ) by 2.4 mbar and the monthly average differed by 0.3 mbar from the standard atmosphere. This would correspond to an AOT error of 0.0014 and 0.000 19, respectively. Thus, with $p(z_0)$ readily available, using standard atmosphere to obtain $p(z_1)$ does not introduce a significant error to $\tau_m(z_1)$. Incidentally, if the lidar absolute calibration is known and the atmospheric density at the altitude z_1 is taken from weather or climatological data, then Eq. (11) can be used to recover AOT from a single elevation angle measurement. However, in practice such absolute calibration is more difficult than performing an elevation scan, or putting it differently, the elevation scan is an easier method to perform such calibration.

To select z_1 we note that in the absence of large volcanic eruptions, concentrations of stratospheric aerosols are normally exceedingly small in comparison to concentrations of tropospheric aerosols. It is therefore safe to assume that the entire vertical column density of aerosols is contained in the altitude range starting from the ground and extending to just above the tropopause. This makes the altitude of a few kilometers above the tropopause a good choice for z_1. At our location the tropopose is located around 10–12 km; thus, we have chosen z_1 = 15 km in our measurements.

The distinct benefit of this measurement over a Langley plot with a sun photometer is that, unlike the sun elevation angle, the lidar elevation scan can be performed quickly, giving more credence to the assumption of constancy (in the integral sense) of the aerosol layer in time and horizontal direction during the measurement.

To quantify the performance of this approach, we performed a 2-week measurement campaign in El Segundo, California, with an elevation-scanning 355-nm lidar that was adapted to this experiment. A collocated Cimel 318 sun photometer collected data simultaneously, and the comparison of these two datasets is the subject of this paper.

3. Experiment

a. Sun photometer

One of the two collocated instruments used in this comparison was a Cimel 318 sun photometer. The sun photometer used is the model standard for the Aerosol Robotic Network AERONET (Holben et al. 1998; NASA 2014). Both calibration and data processing of

the sun photometer are done by NASA's AERONET program. The data used for this study are level 2.0 according to the AERONET classification (NASA 2014).

b. Lidar system and measurement

We adapted an existing 355-nm lidar system to perform this measurement. The actual system used was significantly larger than what would have been ideal; thus, the signal had to be attenuated to avoid saturation. Parameters of a more appropriate system are discussed in the conclusions section below.

The transmitter is based on a frequency-tripled Nd:YAG laser (Spectra Physics model GCR-290), with approximately 370 mJ at 355 nm of transmit energy and a 30-Hz repetition rate (11-W average power). The receiver has an aperture of 0.76 m in diameter, a field stop aperture of 320-μrad in diameter, and a bandpass filter with a 0.3-nm full width at half maximum (FWHM). The signal was further attenuated with neutral density filters to allow photon counting with a photomultiplier (PMT). The angular pointing of the system was calibrated against local landmarks and verified by pointing at the moon. Both were performed with an alignment camera. We estimate the angular pointing accuracy to be better than 0.5°.

The measurement campaign was conducted between 13 and 28 February 2013 in El Segundo. Since we are located about 4 km from the coast, we chose to point our lidar in the azimuth direction approximately parallel to the local coastline of 337° (northwest). Five elevation angles were chosen such that the resulting points are equally spaced on the airmass axis: 80°, 55.9°, 44.1°, 35.8°, and 29.5°. The lidar return signal from 15 km (±0.5 km) altitude was averaged for 3 min (laser-on time) at each elevation angle. Because of communication overheads and manual moving of the lidar elevation angle, the minimum time between successive data points was 5–6 min and the duration of a complete elevation scan was approximately 30 min. To enable comparison with the sun photometer, measurements were performed in the daytime. Therefore, the background was subtracted and then the signal was normalized by laser power as monitored by a photodiode. The typical signal was approximately 4–50 photoelectron counts per laser shot in the 15-km (±0.5 km) altitude range, depending on the elevation angle. This corresponds to 22 000–270 000 photoelectron counts per data point. The background counts ranged from essentially zero after sunset up to 15–30 counts per laser shot in the middle of the day.

4. Lidar data analysis

As expected from Eq. (10), the range-corrected signal $S(\theta)$ depends linearly on the air mass $1/\sin(\theta)$. A representative lidar elevation scan (data point) is shown in Fig. 1, along with the linear fit to the data. The slope found by linear regression is 1.268 ± 0.029 (1σ), which corresponds to $\tau_a + \tau_m(z_1) = 0.634 \pm 0.015$ (1σ). Both angular pointing and the shot noise of the PMT are plotted as error bars. However, the shot noise is smaller than the data point symbols and is obscured by them. The spread of the data points appear to be wider than the error bars, suggesting that uncertainties in the fit are dominated by the variability of the atmosphere rather than the uncertainties associated with measurements at the individual angles.

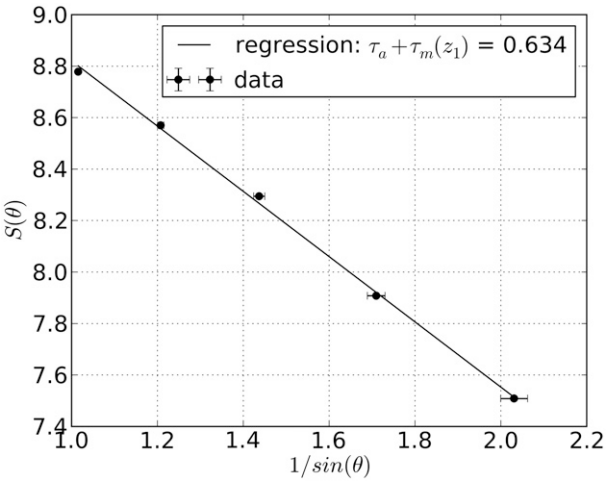

FIG. 1. Representative single measurement showing a range-corrected lidar signal $S(\theta)$ vs air mass $1/\sin(\theta)$. The data were taken at 2252 UTC 26 Feb 2013 in El Segundo, $z_1 = 15$ km, and the coefficient of determination of the regression is $R^2 = 0.9984$.

A large fraction of the total attenuation is due to molecular Rayleigh scattering. We used a Rayleigh 355-nm scattering cross section of 2.7589×10^{-26} cm^2 from Bodhaine et al. (Bodhaine et al. 1999) to obtain a Rayleigh contribution of $\tau_m(z_1) = 0.522$ for $z_1 = 15$ km. We assumed a vertical temperature profile of the standard atmosphere and took the same ground-level pressure as in the AERONET analysis of the sun photometer data. Our choice of pressure was driven by the desire to be as consistent as possible in the analysis of the data from the two instruments. However, we have also tried the analysis with the surface pressure available from a local National Weather Service weather station (available from NOAA NCDC 2013), and we saw essentially the same results in the regression between the time-coincident data from the two instruments.

The other two potential contributors to molecular attenuation are atmospheric NO_2 and ozone. Ozone produces a small correction to the sun photometer measurement at 340 nm (on the order of 0.007). Because the column of ozone is predominantly located in the altitudes

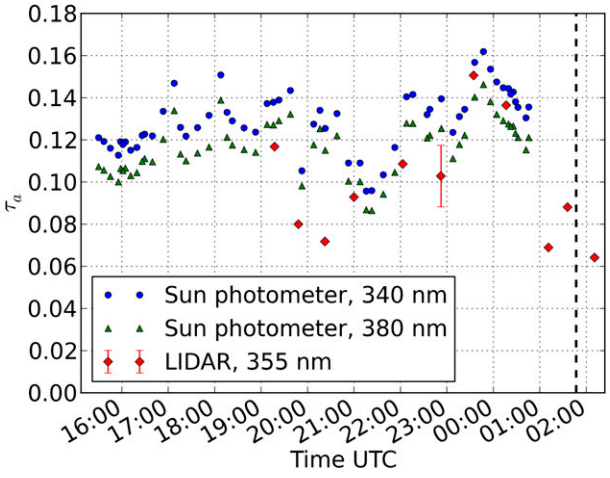

FIG. 2. Time series of lidar AOT at 355 nm and sun photometer AOT at 340 and 380 nm taken at 26 Feb 2013 in El Segundo; sunset at 0147 UTC (dashed line).

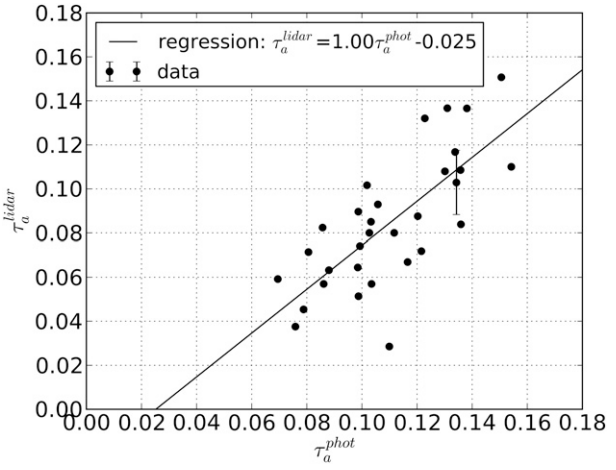

FIG. 3. Scatterplot of lidar AOT vs time-coincident sun photometer AOT at 355 nm for the campaign from 13 to 28 Feb 2013 in El Segundo; $R^2 = 0.55$.

above 15 km and the absorption cross section for ozone is 10 times smaller at 355 than at 340 nm (Sander et al. 2011), no ozone correction has been applied to the lidar data. Note that even in highly polluted environments, where the integrated tropospheric column of ozone may reach 50–60 DU (Fishman et al. 1996), the resulting correction to the lidar-derived AOT would be less than 0.0005. On the other hand, since NO_2 is mostly found below 15 km (Schaub et al. 2006), the lidar AOT was corrected for it. For this comparison experiment, our primary concern was to account for NO_2 consistently between the lidar and the sun photometer. Therefore, we used total column concentrations employed by the AERONET algorithm (Holben et al. 1998; NASA 2014) and applied them to the lidar data. We assumed an NO_2 absorption cross section of 4.562×10^{-19} cm^2 at 355 nm (Harwood and Jones 1994). This resulted in a typical calculated NO_2 absorption contribution of 0.0085 to the total optical thickness. Thus, subtracting these molecular contributions from the total optical thickness gives the lidar AOTs reported in the following section.

5. Results

We conducted a 2-week measurement campaign between 13 and 28 February 2013 in El Segundo, simultaneously collecting data with our elevation-scanning lidar and sun photometer. Several lidar data points (elevation scans) were collected on some days, while none were collected on some others due to weather and other operational constraints. A total of 31 elevation scans were collected. One representative day of measurements (26 February) is shown in Fig. 2. Both lidar AOT and 340- and 380-nm AOT from the sun photometer are shown. Since the values of the sun photometer AOT at the two wavelengths differ by less than 20%, we chose to use a linear interpolation between the two wavelengths to obtain an estimate of AOT at 355 nm for direct comparison with lidar AOT. The standard deviation of the slope found in Fig. 1 is shown as a representative error (1σ).

Time-coincident AOT at 355 nm from the two instruments obtained in this manner are plotted in Fig. 3 as a scatterplot. A linear regression, $\tau_a^{\text{lidar}} = (1.00 \pm 0.17)\tau_a^{\text{phot}} + (0.025 \pm 0.019)$ (1σ), is also shown. The coefficient of determination of this regression is 55%. Again, the standard deviation of the slope found in Fig. 1 is shown as a representative error (1σ). Since the AOT during the campaign stayed in a very narrow range, we consider this to be a good correlation between the two datasets. The fitted slope is also very close to the one-to-one correspondence between the two datasets. The offset, on the other hand, shows statistically significant difference from zero, but it still is within expected uncertainties.

There are potentially three sources of the discrepancy between the two measurements: instrument calibration, Rayleigh optical thickness accuracy, and aerosol layer horizontal nonuniformity. The elevation-scanning lidar AOT measurement is inherently self-calibrating. The sun photometer, on the other hand, depends on periodic absolute calibrations with a transfer standard at NASA on an approximately annual basis. Stability of this absolute calibration is probably the largest source of uncertainty and could explain the 0.025 offset between the two measurements. Holben et al. (1998) reported up to 26% annual decay rate of filter transmission for the two UV channels (380 and 340 nm). They note that this stability was expected to improve with a move to filters made by ion-assisted deposition. However, for our 380- and

340-nm filters, we frequently see 5%–10% annual drifts, which correspond to 0.05–0.1 AOT errors. AERONET performs postdeployment calibration and reanalyzes the data by interpolating between pre- and postdeployment calibrations on an approximately annual basis. The reanalysis assumes linear filter degradation with time. Since the degradation is not necessarily linear, residual offsets remain and get added to the absolute accuracy of the standard, which is used in the calibration. The sun photometer data reported here are corrected with the postdeployment calibration, and the agreement is understandably better. However, the need for the postdeployment recalibration also presents a challenge for rapid measurement campaigns. Clearly, a self-calibrating method such as the lidar approach reported here would be beneficial for such campaigns as well.

In addition to the calibration stability, there are other potential sources of discrepancy between the sun photometer and elevation-scanning lidar data. In the ultraviolet, the contribution to the measured value of $\tau_a + \tau_m(z_1)$ from Rayleigh scattering is much larger than the aerosol contribution, so even a small discrepancy in the Rayleigh cross section can be significant. We chose to use the best available literature value for the cross section (Bodhaine et al. 1999) because the elevation-scanning lidar is an absolute measurement, while the sun photometer measurement is relative to its calibration. Also, all the molecular corrections applied to both sets of raw data, most notably Rayleigh optical thickness and the linear interpolation between the 380- and 340-nm sun photometer channels, are potential contributors to the discrepancy. The offset of 0.025 is only 5% of the calculated Rayleigh optical thickness, so only a small deviation in the Rayleigh correction could account for a significant portion of the offset.

The final potential source of discrepancy is the assumption of horizontal uniformity in the local atmosphere. This point is exacerbated by the coastal location of the measurement. Throughout our measurement campaign, the lidar azimuth pointing was fixed at 337°, which is approximately parallel to the coastline, while the sun photometer derives AOT from direct sun measurement and therefore follows the sun throughout the day, thus pointing in roughly opposite azimuthal direction. As a result, the two instruments may sample somewhat different atmosphere at any given time. However, the data showed no significant correlation with the time of day, which might be expected if this had a large impact on the comparison.

6. Conclusions

We have shown that high-accuracy AOT measurements can be made with an elevation-scanning lidar, even in relatively clear conditions. As the data show, by assuming only horizontal constancy of AOT [independence on elevation angle of the integral in Eq. (9)], we avoided the inaccuracies associated with the assumption of complete aerosol stratification of the conventional multiangle aerosol approach (Adam et al. 2007). The technique has several inherent advantages over the current standard sun photometer method of measuring AOT. The lidar method described here can be made at any time of day (or night) and in any azimuth direction. In addition, the lidar measurement is absolute and thus requires no lengthy pre- and postdeployment calibration. On the other hand, in its current implementation, the lidar method only measures AOT at a single wavelength. While it is possible to expand the lidar system with other wavelengths in the UV and visible, obtaining the same degree of spectral coverage as is achieved by the sun photometer is certainly not very feasible. We therefore see elevation-scanning lidar as a complementary method to the sun photometer technique.

TABLE 1. Possible system specification.

Transmitter	
Pulse energy	4 mJ
Pulse duration	10 ns–10 μs
Receiver	
Aperture diameter	250 mm
Field of view	100 μrad
Spectral bandpass	0.03 nm
PMT quantum efficiency	35%
Optics transmission	35%
Accumulation	5000 laser shots

As mentioned above, the lidar used in this measurement is not representative of the required system parameters. The system can be significantly scaled down without loss of accuracy. In fact, it is easy to imagine a compact micropulse system based on the tripled output of an ytterbium fiber laser (Di Teodoro et al. 2014). For daytime measurement the main challenge would be balancing background light suppression measures with available transmitter pulse energy. High pulse energy presents a challenge for fiber lasers. However, the very relaxed spatial resolution requirement of this measurement permits pulses as long as a few microseconds, thus lowering peak power in the fiber. Nevertheless, additional spectral filtering—for example, with an etalon as was done on CALIPSO (Zaun et al. 2004) and a reduction in the system field of view—would be needed to build a micropulse lidar for daytime operation. Without further commentary possible system parameters are presented in Table 1 for illustration purposes. It should be noted that the parameters in the table are obtained by scaling to match signal and noise collected in our present

measurement, rather than rigorously examining the required signal. Noting that such a laser transmitter can easily operate at a few kilohertz repetition rate, the whole elevation angle scan can be accomplished in just a few minutes.

Acknowledgments. This work was supported by The Aerospace Corporation's Sustained Experimentation and Research for Program Applications and Independent Research and Development programs and NASA Contract NNG11VH00B.

REFERENCES

Adam, M., V. A. Kovalev, C. Wold, J. Newton, M. Pahlow, W. M. Hao, and M. B. Parlange, 2007: Application of the Kano–Hamilton multiangle inversion method in clear atmospheres. *J. Atmos. Oceanic Technol.,* **24,** 2014–2028, doi:10.1175/2007JTECHA946.1.

Adler-Golden, S. M., and J. R. Slusser, 2007: Comparison of plotting methods for solar radiometer calibration. *J. Atmos. Oceanic Technol.,* **24,** 935–938, doi:10.1175/JTECH2012.1.

Alados-Arboledas, L., D. Müller, J. L. Guerrero-Rascado, F. Navas-Guzmán, D. Pérez-Ramírez, and F. J. Olmo, 2011: Optical and microphysical properties of fresh biomass burning aerosol retrieved by Raman lidar, and star-and sun-photometry. *Geophys. Res. Lett.,* **38,** L01807, doi:10.1029/2010GL045999.

Ansmann, A., and D. Müller, 2005: Lidar and atmospheric aerosol particles. *Lidar: Range-Resolved Optical Remote Sensing of the Atmosphere,* C. Weitkamp, Ed., Springer Series in Optical Sciences, Vol. 102, Springer, 105–141.

Bergant, K., A. Filipi, M. Horvat, D. Veberi, D. Zavrtanik, and M. Zavrtanik, 2004: Multiangle lidar approach for estimation of optical thickness and backscatter coefficient ratio of the atmosphere. *Reviewed and Revised Papers Presented at the 22nd International Laser Radar Conference,* G. Pappalardo, A. Amodeo, and B. Warmbein, Eds., Vol. 1, ESA SP-561, 541–544.

Bodhaine, B. A., N. B. Wood, E. G. Dutton, and J. R. Slusser, 1999: On Rayleigh optical depth calculations. *J. Atmos. Oceanic Technol.,* **16,** 1854–1861, doi:10.1175/1520-0426(1999)016<1854:ORODC>2.0.CO;2.

Burton, S. P., R. A. Ferrare, M. A. Vaughan, A. H. Omar, R. R. Rogers, C. A. Hostetler, and J. W. Hair, 2013: Aerosol classification from airborne HSRL and comparisons with the CALIPSO vertical feature mask. *Atmos. Meas. Tech.,* **6,** 1397–1412, doi:10.5194/amt-6-1397-2013.

Di Teodoro, F., P. Belden, P. Ionov, N. Werner, and G. Fathi, 2014: Development of pulsed fiber lasers for long-range remote sensing. *Opt. Eng.,* **53,** 036105, doi:10.1117/1.OE.53.3.036105.

Ferrare, R., and Coauthors, 2006: Evaluation of daytime measurements of aerosols and water vapor made by an operational Raman lidar over the Southern Great Plains. *J. Geophys. Res.,* **111,** D05S08, doi:10.1029/2005JD005836.

Fishman, J., V. G. Brackett, E. V. Browell, and W. B. Grant, 1996: Tropospheric ozone derived from TOMS/SBUV measurements during TRACE A. *J. Geophys. Res.,* **101,** 24 069–24 082, doi:10.1029/95JD03576.

Hair, J. W., and Coauthors, 2008: Airborne High Spectral Resolution Lidar for profiling aerosol optical properties. *Appl. Opt.,* **47,** 6734–6752, doi:10.1364/AO.47.006734.

Hamilton, P., 1969: Lidar measurement of backscatter and attenuation of atmospheric aerosol. *Atmos. Environ.,* **3,** 221, doi:10.1016/0004-6981(69)90010-9.

Harwood, M. H., and R. L. Jones, 1994: Temperature dependent ultraviolet-visible absorption cross-sections of N_2O and N_2O_4: Low-temperature measurements of the equilibrium constant for $2NO_2 \rightleftharpoons N_2O_4$. *J. Geophys. Res.,* **99,** 22 955–22 964, doi:10.1029/94JD01635.

Holben, B. N., and Coauthors, 1998: AERONET—A federated instrument network and data archive for aerosol characterization. *Remote Sens. Environ.,* **66,** 1–16, doi:10.1016/S0034-4257(98)00031-5.

Kahn, R. A., and Coauthors, 2007: Satellite-derived aerosol optical depth over dark water from MISR and MODIS: Comparisons with AERONET and implications for climatological studies. *J. Geophys. Res.,* **112,** D18205, doi:10.1029/2006JD008175.

Kano, M., 1968: On the determination of backscattering and extinction coefficient of atmosphere by using a laser radar. *Pap. Meteor. Geophys.,* **19,** 121–129, doi:10.2467/mripapers1950.19.1_121.

Klett, J. D., 1981: Stable analytical inversion solution for processing lidar returns. *Appl. Opt.,* **20,** 211–220, doi:10.1364/AO.20.000211.

Kokhanovsky, A. A., and G. H. de Leeuw, 2009: *Satellite Aerosol Remote Sensing over Land.* Environmental Sciences, Springer, 388 pp.

Kovalev, V., C. Wold, A. Petkov, and W. M. Hao, 2011: Modified technique for processing multiangle lidar data measured in clear and moderately polluted atmospheres. *Appl. Opt.,* **50,** 4957–4966, doi:10.1364/AO.50.004957.

——, ——, ——, and ——, 2012: Direct multiangle solution for poorly stratified atmospheres. *Appl. Opt.,* **51,** 6139–6146, doi:10.1364/AO.51.006139.

Müller, D., U. Wandinger, D. Althausen, and M. Fiebig, 2001: Comprehensive particle characterization from three-wavelength Raman-lidar observations: Case study. *Appl. Opt.,* **40,** 4863–4869, doi:10.1364/AO.40.004863.

——, A. Kolgotin, I. Mattis, A. Petzold, and A. Stohl, 2011: Vertical profiles of microphysical particle properties derived from inversion with two-dimensional regularization of multiwavelength Raman lidar data: experiment. *Appl. Opt.,* **50,** 2069–2079, doi:10.1364/AO.50.002069.

NASA, 2014: AERONET update. [Available online at http://aeronet.gsfc.nasa.gov/.]

NOAA NCDC, 2013: Quality controlled local climatological data (QCLCD). [Available online at http://cdo.ncdc.noaa.gov/qclcd/QCLCD.]

Pahlow, M., V. A. Kovalev, and M. B. Parlange, 2004: Calibration method for multiangle lidar measurements. *Appl. Opt.,* **43,** 2948–2956, doi:10.1364/AO.43.002948.

Sander, S. P., and Coauthors, 2011: Chemical kinetics and photochemical data for use in atmospheric studies. Evaluation 17, JPL Publ. 10-6, 684 pp. [Available online at http://jpldataeval.jpl.nasa.gov.]

Schaub, D., K. F. Boersma, J. W. Kaiser, A. K. Weiss, D. Folini, H. J. Eskes, and B. Buchmann, 2006: Comparison of GOME tropospheric NO_2 columns with NO_2 profiles deduced from ground-based in situ measurements. *Atmos. Chem. Phys.,* **6,** 3211–3229, doi:10.5194/acp-6-3211-2006.

Shipley, S. T., D. H. Tracy, E. W. Eloranta, J. T. Trauger, J. T. Sroga, F. L. Roesler, and J. A. Weinman, 1983: High spectral resolution lidar to measure optical-scattering properties of atmospheric aerosols. 1: Theory and instrumentation. *Appl. Opt.,* **22,** 3716–3724, doi:10.1364/AO.22.003716.

Sicard, M., P. Chazette, J. Pelon, J. G. Won, and S. C. Yoon, 2002: Variational method for the retrieval of the optical thickness

and the backscatter coefficient from multiangle lidar profiles. *Appl. Opt.,* **41,** 493–502, doi:10.1364/AO.41.000493.

Spinhirne, J. D., J. A. Reagan, and B. M. Herman, 1980: Vertical distribution of aerosol extinction cross section and inference of aerosol imaginary index in the troposphere by lidar technique. *J. Appl. Meteor.,* **19,** 426–438, doi:10.1175/1520-0450(1980)019<0426:VDOAEC>2.0.CO;2.

Sroga, J. T., E. W. Eloranta, S. T. Shipley, F. L. Roesler, and P. J. Tryon, 1983: High spectral resolution lidar to measure optical-scattering properties of atmospheric aerosols. 2: Calibration and data analysis. *Appl. Opt.,* **22,** 3725–3732, doi:10.1364/AO.22.003725.

Zaun, N. H., C. Weimer, Y. Sidorin, and D. Lunt, 2004: Solid-etalon for the CALIPSO lidar receiver. *Earth Observing Systems IX,* W. L. Barnes and J. J. Butler, Eds., International Society for Optical Engineering (SPIE Proceedings, Vol. 5542), 141, doi:10.1117/12.559883.